Desalination and Water Treatment
www.deswater.com

doi:10.5004/dwt.2017.20213

68 (2017) 226–235
March

Efficient removal of different basic dyes using graphene

Muhammad Z. Iqbal[a,d,*], Priyabrata Pal[a], Mohamad Shoaib[a] Ahmed A. Abdala[b,c,*]

[a]*Department of Chemical Engineering, The Petroleum Institute, POB 2538, Abu Dhabi, UAE, email: mziqbal@uaeu.ac.ae (M.Z. Iqbal), ppal@pi.ac.ae (P. Pal), moshoaib@pi.ac.ae (M. Shoaib)*
[b]*Qatar Environment and Energy Research Institute, Hamad Bin Khalifa University, Qatar Foundation, POB 5825, Doha, Qatar,*
[c]*College of Science and Engineering, Hamad Bin Khalifa University, Qatar Foundation, POB 5825, Doha, Qatar, Tel. +974-77963310, Fax + 974 4454 1528, email: aaabdalla@qf.org.qa*
[d]*Department of Chemical and Petroleum Engineering, United Arab Emirates University, Al-Ain, UAE, Tel. +971 3 713 5398, Fax +971 3 762 4262, email: mziqbal@uaeu.ac.ae*

Received 4 June 2016; Accepted 4 September 2016

ABSTRACT

Adsorptive removal of two basic dyes, methylene blue (MB) and malachite green (MG) using thermally reduced graphene (TRG) is reported. TRG was synthesized by thermal exfoliation and reduction of graphite oxide, and characterized by X-ray diffraction, transmission electron spectroscopy, and surface area measurements. The factors affecting the adsorption process such as initial dye concentration, initial solution pH, temperature, and Dye/TRG ratio were investigated. The Dye/TRG ratio was found to be the most important factor controlling the adsorption of MB and MG on graphene surface. Highest adsorption capacity was observed at dye/TRG ratio of 1, irrespective of the initial dye concentration. The maximum measured adsorption capacity of 687 mg/g-TRG for MB and 212 mg/g-TRG for MG, and removal efficiency of 99.62% for MB and 98.74% for MG were obtained. Both dyes followed the Langmuir isotherm indicating the monolayer adsorption on the graphene surface. Thermodynamic analysis indicated the adsorption of MB is an exothermic process whereas adsorption of MG is an endothermic process. In addition, an equilibrium model to model the experimental adsorption data was developed which successfully described the experimental adsorption results and predicted maximum theoretical capacity of 730 mg/g-TRG for MB and 380 mg/ g-TRG for MG, consistent with previously reported results for MB adsorption on graphene and its derivatives.

Keywords: Graphene; Methylene blue; Malachite green; Adsorption; Wastewater treatment

1. Introduction

With the evolution of industrial technology, human health and the environment suffer from various threats. Over the past few decades, stringent environmental policies and regulations related to the emission of industrial waste effluents have been introduced by various regulatory agencies. These regulations require cleaning the wastewater to a level that it is no more hazardous for the living organisms. Textile effluents are regarded as major contributors to the contamination of flowing water. Approximately 10^6 kg/y of dyes are discharged into waste streams by the textile industry [1]. In recent years, continuous efforts towards the production of more stabilized and fast-acting dyes have produced dyes that are difficult to degrade after usage. These developments, though better for the textile industry, have introduced extra risks in effluent discharge and its treatment procedures.

Colored effluents cause serious health and environmental problems by reaching and contaminating the drinking water [2]. Organic components in many of these effluents are biologically non-oxidizable due to their large molecular sizes and structures [1]. Therefore, continuous evolution of the research efforts to bring new developments to treat the colored effluents more effectively are necessary.

Methylene Blue (MB) is a basic dye with a wide range of applications in textile, paper and hair coloring sectors. However, MB causes eye burns for humans and animals in

*Corresponding authors.

addition to various other risks if inhaled [3,4]. Malachite green (MG), another basic dye, is extensively used to dye leather, silk and wool [5]. Though MG was reported to be antiseptic for humans and as antifungal therapeutic agent for animal husbandry, the oral consumption of MG is carcinogenic [6,7]. Moreover, degradation products of MG are also not safe, and possess certain carcinogenic potential [8,9]. Thus, removal of MB and MG dyes from the wastewater is necessary before release into the aquatic environment.

There are various methods to treat colored wastewater containing dyes such as coagulation, oxidation, biological degradation, sonochemical degradation, electrochemical degradation, cation-exchange membranes, and adsorption [8,10–14]. A detailed discussion on the advantages, disadvantages, and selection criteria of dye removal processes is covered in recent reviews [13,17]. Adsorption has a number of advantages due to its low initial cost, flexibility and simplicity of design, ease of operation, and insensitivity towards toxic pollutants [13,18]. In addition, adsorption does not produce any harmful substances after completion of the process cycle, an added advantage. Adsorption has been vastly studied for decontaminating the drinking water with different types of adsorbents originating from natural [19,20], waste [21,22], and synthetic resources [23]. In addition, various adsorbents such as activated carbon [24,25], hazelnut shell [26], perlite [27], clay [28], zeolites [29] are studied for adsorption of MB and MG and some of these adsorbents have shown promising results towards these dyes.

Graphene is a fascinating new member of the carbon allotropic family with honeycomb and one-atom-thick structure. Since its first production, graphene has excited enormous interests during the past several years. Due to the exceptional properties such as very high surface area, electrical conductivity, strength and porous structure, graphene has been studied extensively for its potential applications in various fields [30–35]. The production and applications of graphene are also discussed in detail elsewhere [30,31]. Graphene has shown excellent adsorption characteristics compared to other conventional adsorbents [36–42]. Recently, we have investigated the adsorption of crude oil [43] and methyl orange on graphene [36], and linked graphene microstructure to its adsorption properties.

Graphene oxide is a highly oxidized form of graphene, produced by exfoliating graphite oxide by different methods [30]. Graphite oxide (GO), an un-exfoliated form of graphene oxide, exhibited maximum adsorption capacities of 341 and 248 mg-dye/g-adsorbent for MB and MG, respectively [44]. Similarly, a very high adsorption capacity of approximately 714 mg-MB/g-GO was reported [38]. Liu et al. [37] reported a lower adsorption capacity of 154 mg-MB/g-graphene for reduced graphene, attributed to the lower oxygen contents of reduced graphene.

Thermally reduced graphene (TRG) is produced by simultaneous thermal exfoliation and reduction of graphite oxide [45]. TRG contains C/O atomic ratio ranging from as low as ~7 to a maximum of ~18 with varying surface area and pore characteristics [43,46]. The variation of the C/O ratio imparts an opportunity of tailoring the adsorptive behavior of TRG between that of graphene oxide and pristine graphene.

In this study, TRG was synthesized by thermal exfoliation of GO, and used for adsorptive removal of MB and MG dyes from the aqueous solutions. The adsorption capacity of TRG was measured under various conditions of initial dye concentrations, Dye/TRG ratio, and pH. The equilibrium adsorption data is also studied using adsorption isotherm models. In addition, based on the microstructure of TRG and its equilibrium capacity, we also developed and tested an equilibrium equation to model the experimental adsorption data.

2. Experimental details

2.1. Materials

Methylene blue (purity >97%, microscopy grade, 66720 Sigma Aldrich), malachite green chloride (purity >96%, HPLC grade, 38800 Sigma Aldrich), natural flake graphite (–10 mesh, 99.9%, Alfa Aesar), sulfuric acid (95–97%, J.T. Bakers), hydrochloric acid (37%, Reidel- deHaen), hydrogen peroxide (30% solution, BDH), potassium permanganate and sodium nitrate (Fisher Scientific) and sodium hydroxide (Reidel-deHaen) were used as received.

2.2. Synthesis of TRG

TRG was produced by thermal exfoliation of graphite oxide (GO) [45]. In this method, graphite was oxidized using the Staudenmaier method [47] as follows: graphite (5 g) was placed in ice-cooled flask containing a mixture of H_2SO_4 (90 ml) and HNO_3 (45 ml). Potassium chlorate (55 g) was added slowly to the cold reaction mixture. The reaction was stopped after 96 h by pouring the reaction mixture into water (4 L). 5% HCl solution was used to wash the produced GO until no sulfite ions were detected in the filtrate. The mixture was washed with water till no chloride ions were detected in the filtrate. GO was dried under vacuum overnight. The prepared GO was exfoliated by rapid heating at 1000°C in a tube furnace (Model 21100, Barnstead Thermolyne) under a constant N_2 flow for 30 s.

2.3. Adsorbent characterization

X-ray diffraction (XRD) (X'Pert PRO MPD diffractometer, PANalytical) was used to test the oxidation of graphite, and complete exfoliation of graphite oxide. XRD scan was conducted between 5–35° at a scan rate of 0.02°/s at 40 KV voltage using CuKα radiation of wavelength 1.54 Å. Transmission electron microscopic (TEM) images were obtained using FEI Tecnai G20 TEM with point to point resolution of 0.11 nm. The TEM samples were prepared by dispersing approximately ≈ 0.5 mg of TRG in 25 mL of dimethyl formaamide by sonication for 10 min in a sonicating bath. Two drops of the suspension were deposited on a 400 mesh, copper grid covered with thin amorphous film (lacey carbon). CHN elemental analysis were carried out by Midwest MicroLab. LLC (Indiana, US) using a combustion analyzer at 990°C under ultrapure oxygen, and the determination of oxygen was carried out by Unterzaucher method, separately, at 1050°C. Surface area measurement was conducted at 77 K using Quantachrom Autosorb-1 (Quantachrom Instruments). The sample was degassed for 16 h at 200°C prior to the adsorption measurement. The cumulative pore

volume was determined through BJH cumulative desorption method.

2.4. Adsorption measurements

Batch adsorption experiments were carried out in a 500 mL flask containing 100–400 mL dye solution (100 mL for MG and 400 mL for MB). Typical range of initial dye concentration (C_o mg/L) was from 1.25 to 15 mg/L, and that of TRG dose from 10 to 40 mg. In all the experiments, a stock solution of 1000 mg/L of dyes was prepared, and diluted further for specific measurements. Adsorption was carried out under constant stirring and constant temperature. Small aliquot samples (1.5 ml) were withdrawn from the TRG-dye solutions after the equilibrium was established. The equilibrium concentrations were measured using Genesys™ 20 spectrophotometer (Thermo Electron Corp.) at λ_{max} = 660 nm for MB, and 618 nm for MG. The equilibrium adsorption capacity (q_e, mg-dye/g-TRG) was calculated as $q_e = V(C_o - C_e)/W$, where C_o and C_e (mg/L) are the initial and equilibrium dye concentrations, respectively. V (L) is solution volume, and W (g) is the weight of TRG used. The initial pH of the dye solutions was controlled using 0.1 M NaOH or 0.1 M HCl.

3. Results and discussion

3.1. TRG exfoliation and morphological characterization

The first sign of the oxidation of graphite to GO, and the simultaneous thermal exfoliation and reduction of GO to produce TRG was the substantial increase in the bulk volume from about 1 cm^3/g for graphite and 2 cm^3/g for GO to 150 cm^3/g for TRG. Moreover, the crystallographical structure of GO and TRG as examined by XRD further confirmed the expanded structure of GO, and fully exfoliated TRG (Fig. 1a). Graphite showed an intrinsic (002)-peak at 2θ~26.5° (d-spacing~3.37 Å), that shifted to 2θ~11.4° (d-spacing~7.8Å) in GO. The increase in interlayer spacing in GO and its shift towards lower 2θ is attributed to the presence of the polar oxygen functionalities, and intercalation of water molecules within GO galleries. However, presence of a single peak also indicated that GO still contained the ordered structure. It is worth noting that the graphite (002)-peak was much narrower, and exhibited a much higher intensity than GO (002)-peak, indicating the less ordered structure in GO compared to that in graphite. On the other hand, no noticeable diffraction peaks were observed for TRG, confirming the complete exfoliation of GO and the presence of no ordered/stacked layers in TRG.

TEM morphology (Fig. 1b) showed that TRG was comprised of thin paper-like sheets extending over 2 μm in lateral dimension. The sheet edges appeared as dark fields due to the overlapping and folding edges. The thin, layered structure was another evidence of the complete exfoliation of GO into TRG. Nevertheless, TRG surface was wrinkled, attributed to the presence of residual oxygen-moieties left after the thermal exfoliation process. These wrinkles resulted in contrast difference in the image, showing nano-sheets less transparent than the actual [48].

Type-II adsorption-desorption isotherm for TRG was observed from the BET measurement at 77K (inset in Fig. 2). The type-II adsorption represents the aggregated plate-like particles with slit-shaped pores [49]. Graphene exhibited multilayer adsorption until a high P/Po was reached due to the delayed capillary condensation (Fig. 2). On the other hand, during desorption process, the state of adsorbate changed, following a different path than adsorption until a critical value of P/P_o was reached, where the adsorption-desorption curves re-converged. The pore volume, pore size distribution, and surface area of TRG were determined using the BJH desorption method [36]. The TRG sample exhibited a cumulative pore volume and surface area of 1.34 cm^3/g and 486 m^2/g, respectively. The observed surface area of TRG appeared less than the one normally exhibited by graphene, which could be attributed to the highly reduced nature of TRG that might result in some re-stacking of the nano-sheets. The pore size distribution showed that

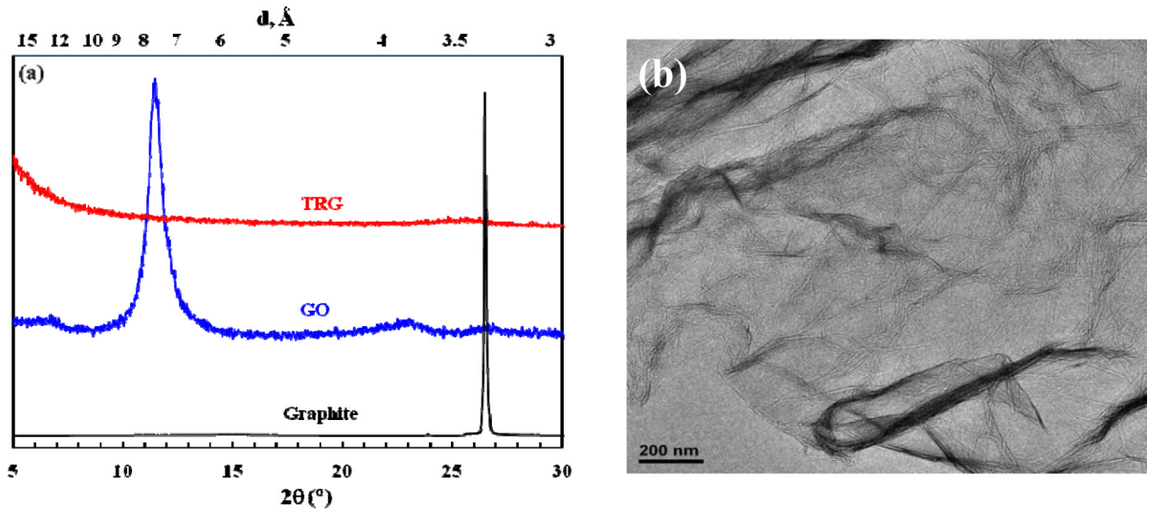

Fig. 1. (a). XRD patterns of graphite, graphite oxide and TRG and (b) TEM image of TRG.

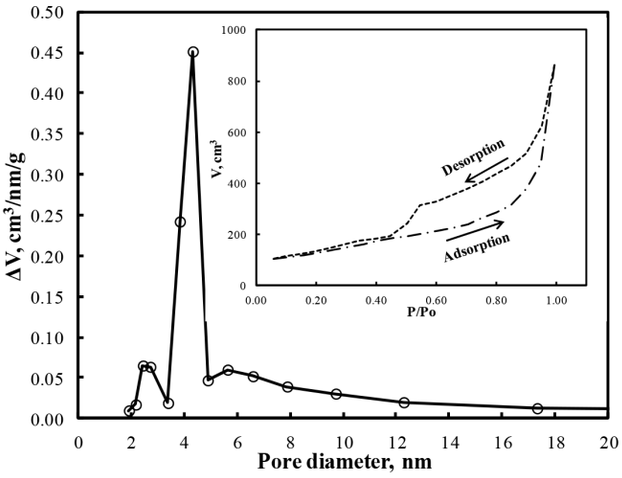

Fig. 2. Pore size distribution of TRG. Inset shows adsorption-desorption isotherm.

TRG was composed of meso-pores (2 nm < d < 50 nm) and no micropores (<1 nm) were observed.

3.2. Adsorption analysis

The effects of various adsorption process variables such as temperature, pH, initial dye concentration, and Dye/TRG ratio on the adsorption capacity were examined.

The C_o (for both MB and MG) was varied from 5 to 20 mg/L with a fixed TRG loading (10 mg) (Fig. 3). Increasing C_o led to an increase in equilibrium adsorption capacity (q_e, mg/g), and decrease in % removal. Specifically, a slight decrease in % removal was observed for MB (98.4% to 86%), whereas a slightly higher decrease was observed for MG (96% to 76%) in the same range of the tested C_o (5 to 20 mg/L). Meanwhile, the equilibrium adsorption, q_e increased from 197 mg/g to 687 mg/g for MB (~350% increase), and from 48 mg/g to 141 mg/g for MG (~300% increase) with increasing C_o. The elemental analyses showed that C/O atomic ratio of TRG sample was 11/1, which was above the typical value of 10/1 observed for thermally and chemically reduced graphene (showing a more reduced form of TRG). Recently, FTIR [36], XPS and NMR [50] studies confirmed the presence of epoxy, hydroxyl and carbonyl groups on reduced graphene. The presence of oxy-groups was also observed to enhance the adsorption capacity of the adsorbent [38]. The observed adsorption capacity of MB on TRG was in between that of graphene oxide, 714 mg/g [38], and highly reduced graphene 153 mg-MB/g-TRG [37], which also signifies the role of oxygen contents on graphene surface in the adsorption. The decrease in removal % is attributed to the increased number of dye molecules in solution, making graphene surface less accessible to the dye molecules attaching after the first monolayer.

Textile effluents normally exhibit different pH. Therefore, the effectiveness of adsorbent should also be linked with changing pH for better control and understanding of adsorption process. Within the studied pH of 3.5 to 11, the removal efficiency increased from 77.5% to 99.4% for MB, and from 93.2% to 99.9% for MG (Fig. 4). The q_e increased from 620 mg/g to 796 mg/g for MB, and from 140 mg/g to 150 mg/g for MG for the same pH change, respectively. Thus, the basic environment accelerated TRG's performance for both dyes, which was also observed for reduced graphene and graphene oxide [37,38]. However, TRG showed better adsorption capacity and % removal than that reported for the reduced graphene, attributed to the presence of oxy-groups on TRG surface that enhanced the surface complexation, and further helped in an early attainment of the equilibrium. Compared with MB, the MG's adsorption capacity became nearly stagnant after the pH of 4.5. As reported by Samiey and Toosi [51], under alkaline conditions, MG transforms into carbinol-base containing – OH functional group at the junction of three

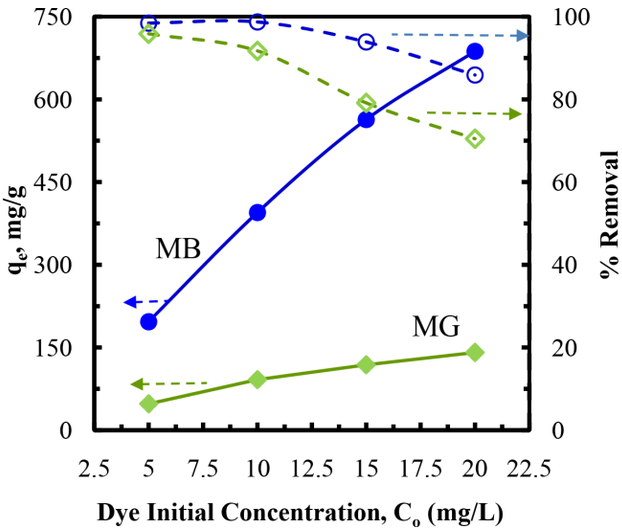

Fig. 3. Effect of initial dye concentration on equilibrium adsorption capacity (closed symbol) and % removal (open symbols) for MB (blue circles) and MG (green squares). Data reported at T = 22°C, pH = 6.7, and TRG = 10 mg.

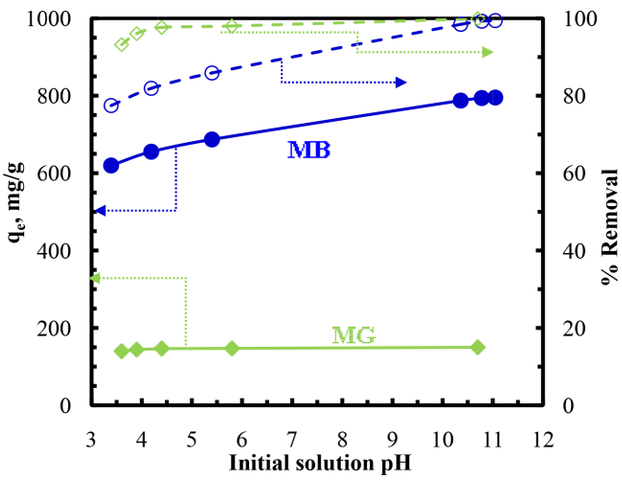

Fig. 4. Effect of initial pH on equilibrium adsorption capacity (closed symbol) and % removal (open symbols) for MB (blue circles) and MG (green squares). Data reported at T = 22°C, TRG = 10 mg, C_o for MB = 20 mg/L, and C_o MG = 15 mg/L

benzenic rings of MG. In addition, the MG molecules containing positive charges in the solution, get neutralized under basic conditions. Thus, the electrostatic forces of attraction between TRG and MG are reduced due to the neutralization reaction, and eventually, a slow uptake of MG was observed with increasing pH. Nevertheless, a detailed analysis of the transformation of MG in solution in the presence of graphene with changing pH might give a better understanding of the adsorption stagnation at higher pH.

Optimization of the adsorption process using minimum adsorbent dose to clean the maximum amount of colored water is most pertinent in adsorbent design. Here, the optimization has been carried out by altering Dye/TRG ratio at fixed dye initial concentrations. Strong effects of adsorbent dosage on the adsorption process are well established. However, here, we show that it is not the adsorbent dosage that has a direct effect on the adsorption capacity, but the Dye/adsorbent ratio, which determined by the dye concentration, and the liquid to solid volume, has the prime importance. Fig. 5 shows the effect of Dye/TRG ratio on q_e, and % removal for both MB and MG dyes. The Dye/TRG ratio was changed from 0 to 1 by maintaining a constant C_o, and changing the TRG dosage in the solution. Similarly, measurements were conducted at various fixed C_o values for both dyes. q_e was directly proportional to Dye/TRG ratio irrespective of C_o value in solution (Fig. 5a). There was an increasing trend in q_e with increasing the Dye/TRG ratio. This was a striking result because dye adsorption is considered as a concentration-gradient-based diffusion process, where the adsorption capacity should increase with increasing dye concentration [37] (see Fig. 3). However, fixing Dye/TRG ratio did not affect the adsorption capacity, revealing adsorption dependent on the Dye/adsorbent number of contacts and not on C_o alone. In case of methyl orange adsorption on TRG [36] at fixed Dye/TRG ratio, changing C_o altered the adsorption capacity non-linearly. However, this is not the case here. Increasing Dye/TRG ratio decreased the removal % for both MB and MG. In general, at Dye/TRG > 1, more dye molecules are present in solution compared to TRG, resulting in decreased removal %. This behavior can also be attributed to the fact that adsorption of MB and MG is a strong function of number of ionic sites on the adsorbent.

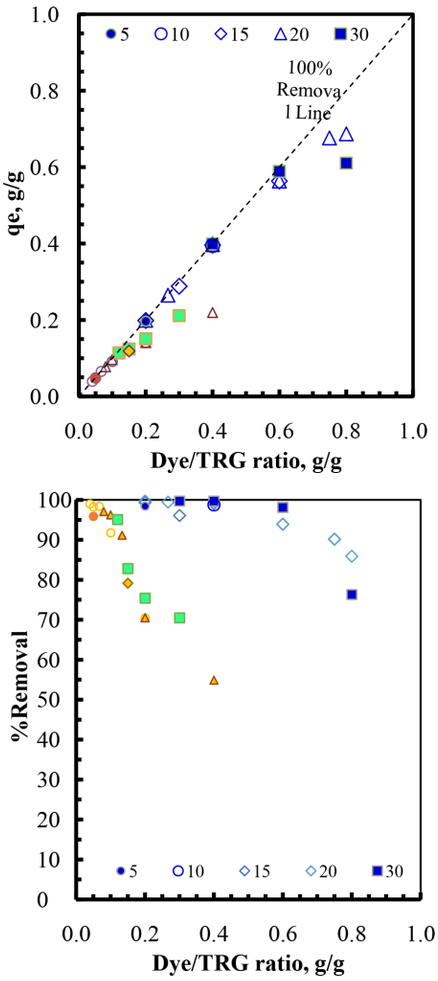

Fig. 5. Effect of dye/TRG ratio on q_e (a) and % removal (b) for MB and MG (the color schemes in 'a' and 'b' are the same).

Adsorption from dilute solution can be regarded as an exchange process where molecules can adsorb not because of ionic attraction towards solid surface, but also due to rejection from the solution [52]. Solvents in adsorption from dilute solution are called the structureless continuum [53] which leads to applying typical gas adsorption equations directly onto the liquids by replacing the pressure with concentration. The experimental data analyzed using equilibrium isotherms helps extracting information about molecular interactions between the adsorbate and adsorbents. On the other hand, non-idealities in dilute solutions can also lead to non-ideality in isotherms [52]. Various types of isotherms have been reported to explore different aspects of adsorption process [54].

The Langmuir isotherm essentially assumes monolayer distribution of adsorbate on finite adsorption sites with uniform energies having no lateral interactions and steric hindrance between the adsorbate molecules even on adjacent sites [55]. Mathematically, the Langmuir isotherm is shown in Eq. (1) in non-linear form:

$$q_e = \frac{bC_e}{1 + q_m C_e} \tag{1}$$

where q_m is the maximum adsorption capacity, C_e is the equilibrium concentration and b is the Langmuir constant. The Langmuir constant, b is related to rate of adsorption. A linear form of Eq. (1) is given by:

$$\frac{C_e}{q_e} = \frac{1}{q_m b} + \frac{C_e}{q_m} \tag{2}$$

Another important parameter, R_L, the separation factor [56] can be extracted from Langmuir isotherm defined as follows:

$$R_L = \frac{1}{1 + bC_{o,m}} \tag{3}$$

Here $C_{o,m}$ is the maximum initial concentration of the dye used in the Langmuir analysis. The R_L is a qualitative measure of the adsorption process favorability such that $R_L = 1$

indicates unfavorable process, $0 < R_L < 1$ indicates favorable, $R_L = 0$ indicates irreversible process.

Non-ideal and reversible adsorption can be expressed using the Freundlich isotherm [57] which assume multilayer adsorption over a heterogeneous surface. The non-linear and linear forms of Freundlich model are given by Eqs. (4) and (5), respectively:

$$q_e = K_F C_e^{1/n} \tag{4}$$

$$\ln q_e = \ln K_F + \frac{1}{n}\ln C_e \tag{5}$$

Typical range of slope ($1/n$) in Eq. (5) is from 0 and 1, and measures the adsorption intensity or the surface heterogeneity (more heterogeneous surface as slope approached zero). Moreover, the slope ($1/n$) <1 implies chemisorption process, and >1 indicates cooperative adsorption [58].

Parts a and b of Fig. 6. shows linear fitting of the experimental data to the Langmuir and Freundlich isotherm models for C_o changing from 5 to 20 mg/L at room temperature. Both, MB and MG were observed to follow the Langmuir isotherm (R^2~1). The Langmuir model predicted the maximum adsorption capacity, q_m of 727 and 151 mg-dye/g-TRG

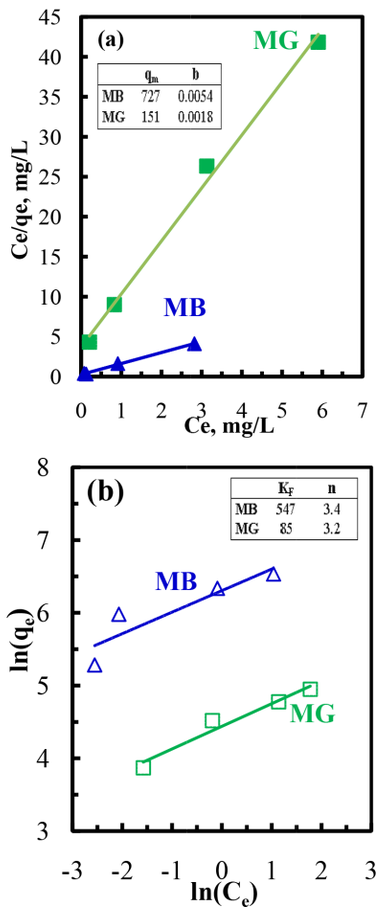

Fig. 6. Fitting of the adsorption data to Langmuir (a), and Freundlich (b) isotherm

for MB and MG, respectively, in agreement with the experimental data (Fig. 3). The Langmuir constant, b was used to calculate R_L using the maximum C_o utilized in fitting as 20 mg/L. In this work, R_L was found to be close to 1 (0.90 for MB and 0.97 for MG), indicating favorable adsorption. On the other hand, the Freundlich isotherm under predicted the maximum adsorption capacity for both dyes (K_F ~ 547 for MB and 85 for MG), showing the incapability of the Freundlich isotherm in modeling these dyes. Also, the Freundlich constant, n, calculated from the linear fits for both dyes was above 1. Typically, as n decreases, adsorption becomes more difficult. In general, good adsorption is observed for n = 2–10, difficult adsorption n = 1–2 and for poor adsorption n is less than 1. In our case, the value of n was in the range of good adsorption, and these was no other significant piece of information that could be extracted from the Freundlich isotherm.

For thermodynamic analyses [36] in the temperature range of 2575°C (Fig. 7), a highly reduced form of TRG was used with high C/O ratio in order to compare our observation with the results from Ref. [37]. The adsorption capacity of MB decreased with increasing temperature, indicating exothermic adsorption. On the other hand, the increased adsorption of MG with increasing temperature showed endothermic behavior. The change in Gibb's free energy (ΔG°) was calculated using the expression [36,59]: $\Delta G° = -RT\ln(k_d)$, where k_d is the distribution constant for the equilibrium sorption, calculated as $k_d = q_e/C_e$. The calculated ΔG° increased from –7.7 to –6.3 for 22 and 57°C for MB, whereas for MG, the ΔG increased from 24.3 to 83.6 KJ/mol for 22 and 74°C, respectively. Furthermore, the Van't Hoff equation was used to calculate the averaged standard enthalpy change (ΔH°), and standard entropy change (ΔS°) as follows: $ln(k_d) = -\Delta H°/RT + \Delta S°/R$, where T is the absolute temperature (K), and R is the universal gas constant (8.314 J mol^{-1} K^{-1}). A straight line between $\ln(k_d)$ and T gives ΔS° from the intercept, and ΔH° is obtained from the slope. The ΔH° was found to be –20.4 and 19.7 KJ/mol for MB and MG, and ΔS° values were –43.6 and 85 J/mol K for MB and MG, respectively. The thermodynamic parameters such as ΔG° and ΔH° are considered important in predicting and understanding nature of the adsorption process. A highly negative ΔG° value for MB indicated a spontaneous adsorption, whereas MG exhibited a highly positive ΔG°, showing difficult adsorption on TRG surface. Similarly, ΔH° was negative for MB but positive for MG. A Similar endothermic adsorption of MG was reported for zeolites [60], and surface modified phyllosilicates [61]. A negative ΔS° for MB further indicates ordered adsorption, whereas a positive ΔS° for MG indicates random arrangement of MG molecules on graphene surface [62].

3.3. Equilibrium model development

For further analyses of the adsorption on graphene, an equilibrium-based expression has been developed to understand the nature of the adsorption process. The dye-TRG equilibrium adsorption process can be described as follows:

$$TRG + xDye \rightleftharpoons TRG - Dye_X \tag{6}$$

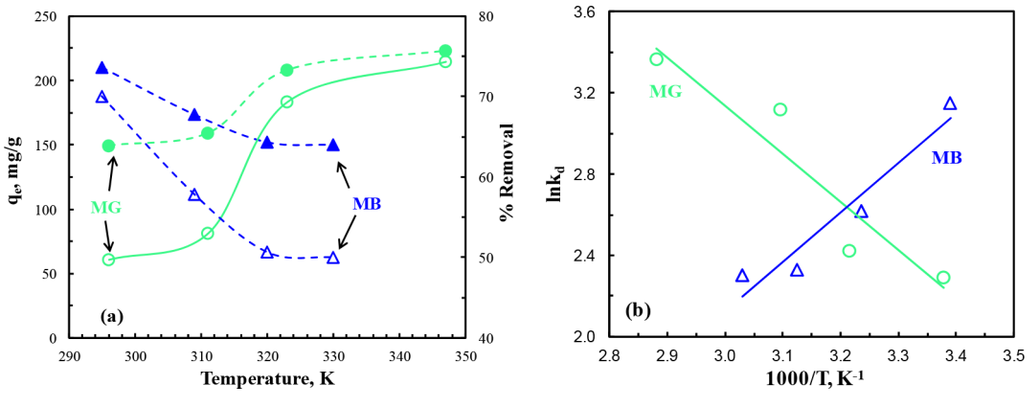

Fig. 7. Effect of temperature on adsorption behavior of MB and MG (a) and thermodynamic analysis. Open symbols in (a) represent %removal and closed symbols represent q_e.

Here "x" is the stoichiometric Dye/TRG ratio (g/g), TRG is the amount of unsaturated graphene, TRG-Dye_x is the sum of the saturated TRG and the adsorbed dye.

Thus, the mass equilibrium constant, K, for such equilibrium process is given by:

$$K = \frac{TRG - Dye_x}{[TRG][Dye]^x} \tag{7}$$

Let the fraction of the saturated TRG = y, the amount of adsorbed dye per gram of initial TRG, q_e, can be given as:

$$q_e = \frac{\text{adsorbed dye}}{\text{initial TRG}} = xy \tag{8}$$

At equilibrium,

$$\text{Amount of unsaturated TRG, } [TRG] = [TRG]_0(1-y)$$

$$\text{Amount of unadsorbed dye, } [dye] = [dye]_0 - [TRG]_0 xy = [TRG]_0(\theta - xy)$$

$$\text{Sum of saturated TRG and adsorbed dye, } [TRG - Dye_x] = [TRG]_0(y + xy)$$

Taking a basis of 1 g of initial TRG dose,

$$K = \frac{TRG - Dye_x}{[TRG][dye]^x} = \frac{y + xy}{(1-y)(\theta - xy)^x} \tag{9}$$

$$K = \frac{q_e(1+x)}{(x - q_e)(\theta - q_e)^x} \tag{10}$$

Since x is constant, and K is the only function of T and pH, the model predicts that adsorption capacity, q_e, is only a function of the initial Dye/TRG ratio (θ) as indicated by Eq. (10). This is consistent with our experimental results shown in Fig. 8, where q_e data obtained from experiments with different C_o collapse on one curve when plotted against the Dye/TRG ratio.

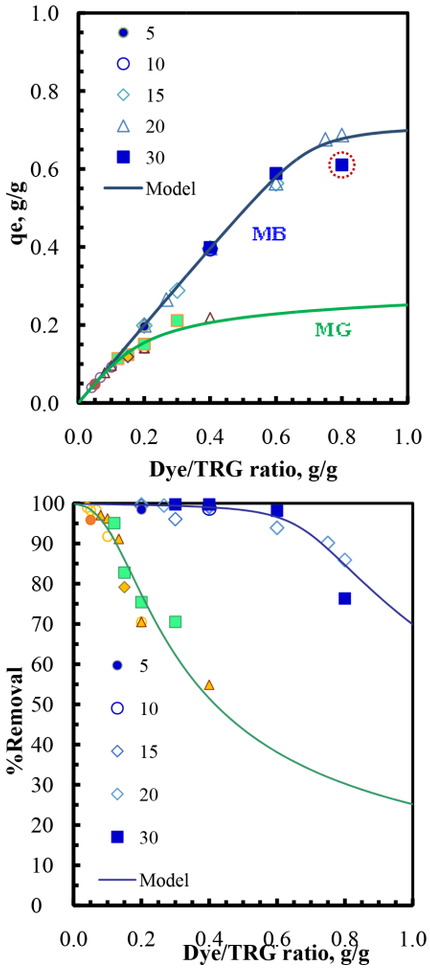

Fig. 8. Comparison of experimental and model calculated adsorption capacities.

In order to determine the model parameters (K and x), we used experimental data presented above. An excel solver function was used that assumes values for K and x, and recalculates K from Eq. (10) at each data point. The solver

Table 1
Model parameters for adsorption of MB and MG on TRG

	MB	MG
K	115.4	0.73
x, mg/g	730	380

function searches for a solution that minimizes $\sum(K_{assumed} - K_{calculated})^2$. The model was then used to fit the experimental data using a goal seek function that calculates q_e at each data point using the K and *x* values obtained from the solver function (Table 1).

The equilibrium constant, K for MB was calculated to be 115.4, and that for MG was 0.73, whereas the value of *x* was 730 mg/g (0.73 g/g) for MB, and 380 mg/g (0.38 g/g) for MG. The very high K value for MB indicated higher affinity of TRG towards MB compared to MG. A small value of K (K = 0.73) for MG might indicate that MG did not completely follow a single layer adsorption as observed in the Langmuir analyses. MG might form complexes on TRG surface, which would restrict its further adsorption on the graphene. We plotted the experimentally determined q_e versus Dye/TRG ratio (θ, g/g) in Fig. 8. The value of *x* signifies the maximum theoretical adsorption capacity. This capacity can be achieved experimentally when a very high dye/TRG ratio is used whereas the actual adsorption capacity is a function of feed Dye/TRG ratio. In order to validate the developed model, we compared the recently published data with model predictions. The feed Dye/TRG ratio used by Yang et al. [38] was 0.533 g/g, which was very low compared with our experiments. However, the reported maximum adsorption capacity was 0.714 g/g (714 mg/g) for MB, which is the highest reported adsorption capacity for graphene oxide. However, it iss still slightly below the theoretical maximum (*x* = 0.73 g/g). We believe that this high adsorption capacity was due to the high contents of oxygen-pendant groups on the graphene oxide surface. Liu et al. [37] reported the adsorption of MB on graphene using Dye/TRG = 0.055–0.2 g/g, and obtained an adsorption capacity of ~80 to 180 mg/g, respectively. Our model predicts an adsorption capacity of 50 mg/g for θ = 0.05, and 199 mg/g for θ = 0.2, validating the equilibrium model. Ramesha et al. [63] used exfoliated GO for adsorbing MB and used a Dye/adsorbent ratio of 0.23 g/g to obtain an adsorption capacity of 17.3 mg/g, which is extremely low compared to this study and other reports. Based on the comparison of our model predictions with the published reports, it is reasonable to believe that this model can describe adsorption of MB on graphene very successfully. On the other hand, there was a single report on MG adsorption by graphene oxide [64] and the feed Dye/adsorbent ratio was not provided. That's the reason, we could not compare our results with others for MG adsorption at this time.

We also compared the adsorption capacities of various graphene-based adsorbents for MB adsorption (Table 2). There were varying adsorption capacities reported for graphene oxide [38,63,65,66], which might be attributed to the preparation methods for graphene, and the feed Dye/adsorbent ratio being used. The influence of adsorbent preparation method also affected the surface area of the adsorbents in these studies. In addition, the attachment of various materials on graphene surface might have reduced the accessible surface area of graphene to dye molecules, which was exhibited by the lower adsorption capacity of graphene nanosheet/Fe_2O_3, chitosan-graphene oxide, and

Table 2
Comparison of adsorption capacities of various graphene-based adsorbents

Adsorbent	Surface area (m^2/g)	Dye	Feed dye/adsorbent ratio (g/g)	Max Removal %	Adsorption capacity (mg/g)
Graphene oxide [38]	N/A	MB	0.5	99%	714
Graphene oxide [65]	32	MB	0.4	99.6%	241
Graphene oxide [64]	28.5	MB	N/A	N/A	224
Graphene oxide [66]	N/A	MB	0.1	N/A	43.5
Graphene [37]	296	MB	0.2	99%	351
Exfoliated graphite oxide [63]	N/A	MB	0.04	100%	17
Graphene nanosheet [67]	N/A	MB	0.06	N/A	60
Graphene nanosheets/ Fe_3O_4 composites [67]	N/A	MB	0.06	64%	35
Magnetic Chitosan-graphene oxide [66]	392	MB	0.1	N/A	46
Graphene/CNT composites [68]	79	MB	0.07	97%	82
Thermally reduced graphene (current study)	486	MB	0.05–0.8	99.62%	687
Thermally reduced graphene (current study, prediction)	486	MB	0.05–1.0	99.71%+	730+
Graphene oxide [64]	28.5	MG	N/A	N/A	248
Thermally reduced graphene (current study)	486	MG	0.05–0.4	98.97%	212
Thermally reduced graphene (current study, prediction)	486	MG	0.05–1.0	98.43%+	380+

+Model prediction

graphene/carbon nanotube composites [66–68]. Overall, in comparison, the adsorption capacity of TRG for MB and MG dyes has been fairly reasonable compared with other graphene-based adsorbents.

4. Conclusions

We have used TRG for adsorptive removal of MB and MG from the aqueous solutions. Increasing initial dye concentration increased adsorption capacity, which further increased under the basic environment. The Dye/TRG ratio was found to be the most pertinent factor in controlling adsorption capacity of TRG in solution. The highest adsorption capacity was observed at Dye/TRG ratio of 1 irrespective of the initial dye concentration, indicating that Dye/TRG ratio can be used as a scaling parameter. The Langmuir isotherm successfully predicted the maximum adsorption capacities for both dyes with monolayer adsorption. In addition, an equilibrium equation and equilibrium constant expression was developed to predict the maximum allowable adsorption capacity of graphene. A comparison of model and experimental adsorption capacities revealed that MB had more affinity towards graphene than MG. However, the model still needs more work to include the chemistry of the dyes and that of adsorbent surface. Further investigation will reveal a more generalized picture of the adsorption process on the molecular level.

Acknowledgement

The authors would like to thank Dr. Marios Katsiotis and Jamie Whelan (The Petroleum Institute, Abu Dhabi) for their assistance in TEM and BET analysis, respectively.

References

[1] K.K.H. Choy, G. McKay, J.F. Porter, Sorption of acid dyes from effluents using activated carbon, Resour. Conserv. Recy., 27 (1999) 57–71.
[2] K. Slater, Environmental impact of textiles: production, processes and protection: Woodhead Publishing; 2003.
[3] S. Senthilkumaar, P. Varadarajan, K. Porkodi, C. Subbhuraam, Adsorption of methylene blue onto jute fiber carbon: kinetics and equilibrium studies, J. Colloid. Interf. Sci., 284 (2005) 78–82.
[4] C.A. Gruetter, P.J. Kadowitz, L.J. Ignarro, Methylene blue inhibits coronary arterial relaxation and guanylate cyclase activation by nitroglycerin, sodium nitrite and amyl nitrite, Can. J. Physiol. Pharmacol., 59 (1981) 150–156.
[5] J. Zhang, Y. Li, C. Zhang, Y. Jing, Adsorption of malachite green from aqueous solution onto carbon prepared from Arundo donax root, J. Hazard. Mater., 150 (2008) 774–782.
[6] A. Mittal, Adsorption kinetics of removal of a toxic dye, Malachite Green, from wastewater by using hen feathers, J. Hazard. Mater., 133 (2006) 196–202.
[7] S. Nethaji, A. Sivasamy, G. Thennarasu, S. Saravanan, Adsorption of Malachite Green dye onto activated carbon derived from Borassus aethiopum flower biomass, J. Hazard. Mater., 181 (2010) 271–280.
[8] S. Singh, M. Das S.K. Khanna, Biodegradation of Malachite Green and Rhodamine B by Cecal Microflora of Rats, Biochem. Biophys. Res. Commun., 200 (1994) 1544–1550.
[9] S.J. Culp, L.R. Blankenship, D.F. Kusewitt, D.R. Doerge, L.T. Mulligan, F.A. Beland, Toxicity and metabolism of malachite green and leucomalachite green during short-term feeding to Fischer 344 rats and B6C3F 1 mice, Chem-Biol. Interact., 122 (1999) 153–170.
[10] W. Chu, Dye removal from textile dye wastewater using recycled alum sludge, Water. Res., 35 (2001) 3147–3152.
[11] N. Azbar, T. Yonar, K. Kestioglu, Comparison of various advanced oxidation processes and chemical treatment methods for COD and color removal from a polyester and acetate fiber dyeing effluent, Chemosphere, 55 (2004) 35–43.
[12] Y. Iida, T. Kozuka, T. Tuziuti, K. Yasui, Sonochemically enhanced adsorption and degradation of methyl orange with activated aluminas, Ultrasonics, 42 (2004) 635–639.
[13] M. Rafatullah, O. Sulaiman, R. Hashim, A. Ahmad , Adsorption of methylene blue on low-cost adsorbents: A review, J. Hazard. Mater., 177 (2010) 70–80.
[14] V.K.G. Suhas, Application of low-cost adsorbents for dye removal - A review, J Environ. Manage., 90 (2009) 2313–2342.
[15] G. Crini, Non-conventional low-cost adsorbents for dye removal: a review, Bioresour. Technol., 97 (2006) 1061–1085.
[16] E. Forgacs, T. Cserháti, G. Oros, Removal of synthetic dyes from wastewaters: a review, Environ. Int., 30 (2004) 953–971.
[17] G.Z. Kyzas, E.A. Deliyanni, K.A. Matis, Graphene oxide and its application as an adsorbent for wastewater treatment, J. Chem. Technol. Biotechnol., 89 (2014) 196–205.
[18] V.K. Garg, Green chemistry for dyes removal from waste water, Green Processing Synth., 4 (2015) 507–508.
[19] S. Sadaf, H.N. Bhatti, S. Nausheen, M. Amin, Application of a novel lignocellulosic biomaterial for the removal of Direct Yellow 50 dye from aqueous solution: Batch and column study, J. Taiwan. Inst. Chem. Eng., 47 (2015) 160–170.
[20] S. Sadaf, H.N Bhatti, M. Arif , M. Amin, F. Nazar, Adsorptive removal of direct dyes by PEI-treated peanut husk biomass: Box–Behnken experimental design, Chem. Ecol., 31 (2015) 252–264.
[21] A. Mittal, L. Kurup, Column operations for the removal and recovery of a hazardous Dye Acid Red-27 from aqueous solutions using waste materials-bottom ash and de-oiled soya, Ecol. Environ. Conserv., 12 (2006) 181.
[22] A. Mittal, J. Mittal, Hen feather: A remarkable adsorbent for dye removal, In: S. K. Sharma, Green Chemistry for Dyes Removal from Wastewater: Research Trends and Applications, John Wiley & Sons, Inc. (2015).
[23] G. Sharma, M. Naushad, D. Pathania, A. Mittal, G. El-Desoky, Modification of Hibiscus cannabinus fiber by graft copolymerization: Application for dye removal, Desal. Wat. Treat., 54 (2015) 3114–3121.
[24] M. Hema, T. Rajachandrasekaran, S. Arivoli, Adsorption kinetics and thermodynamics of Malachite green dye onto acid activated low cost carbon, Int. J. Sci. Res., 17 (2008) 75–87.
[25] B.H. Hameed, A.T.M. Din, A.L. Ahmad, Adsorption of methylene blue onto bamboo-based activated carbon: Kinetics and equilibrium studies, J. Hazard. Mater., 141 (2007) 819–825.
[26] M. Dogan, H. Abak, M. Alkan, Adsorption of methylene blue onto hazelnut shell: Kinetics, mechanism and activation parameters, J. Hazard. Mater., 164 (2009) 172–181.
[27] B. Acemioglu, Batch kinetic study of sorption of methylene blue by perlite, Chem. Eng. J., 106 (2005) 73–81.
[28] A. Gürses, S. Karaca, C. Dogar, R. Bayrak, M. AçIkyIldIz, M. YalçIn, Determination of adsorptive properties of clay/water system: methylene blue sorption, J. Colloid. Interf. Sci., 269 (2004) 310–314.
[29] S. Sohrabnezhad, A. Pourahmad, Comparison absorption of new methylene blue dye in zeolite and nanocrystal zeolite, Desalination, 256 (2010) 84–89.
[30] Y. Zhu, S. Murali, W. Cai, X. Li, J.W. Suk, J.R. Potts, R.S Ruoff, Graphene and graphene oxide: Synthesis, properties, and applications, Adv. Mater., 22 (2010) 3906–3924.
[31] H. Kim, A.A. Abdala, C.W. Macosko, Graphene/polymer nanocomposites, Macromolecules, (2010).
[32] A. Geim, K. Novoselov, The rise of graphene, Nat. Mater., 6 (2007) 183–191.
[33] A. Geim, Graphene: status and prospects, Science, 324 (2009) 1530.

[34] M.Z. Iqbal, A.A. Abdala, V. Mittal, S. Seifert, A.M. Herring, M.W. Liberatore, Processable conductive graphene/polyethylene nanocomposites: Effects of graphene dispersion and polyethylene blending with oxidized polyethylene on rheology and microstructure, Polymer, 98 (2016) 143–155.
[35] H. Alhumade, A. Abdala, A. Yu, A. Elkamel, L. Simon, Corrosion inhibition of copper in sodium chloride solution using polyetherimide/graphene composites, Can. J. Chem. Eng., 94 (2016) 896–904. .
[36] M.Z. Iqbal, A.A. Abdala, Thermally reduced graphene: synthesis, characterization and dye removal applications, RSC Adv., 3 (2013) 24455–24464.
[37] T. Liu, Y. Li, Q. Du, J. Sun, Y. Jiao, G. Yang, Z. Wang, Y. Xia, W. Zhang, K. Wang, H. Zhu, Adsorption of methylene blue from aqueous solution by graphene, Colloid Surf. B, 90 (2011) 197–203.
[38] S.T. Yang, S. Chen, Y. Chang, A. Cao, Y. Liu, H. Wang, Removal of methylene blue from aqueous solution by graphene oxide, J. Colloid. Interf. Sci., 359 (2011) 24–29.
[39] Y. Zhang, H.L. Ma, J. Peng, M. Zhai, Z.Z. Yu, Cr (VI) removal from aqueous solution using chemically reduced and functionalized graphene oxide. J. Mater. Sci., 48 (2013) 1883–1889.
[40] D. Robati, B. Mirza, M. Rajabi, O. Moradi, I. Tyagi, S. Agarwal V.K. Gupta, Removal of hazardous dyes-BR 12 and methyl orange using graphene oxide as an adsorbent from aqueous phase, Chem. Eng. J., 284 (2016) 687–697.
[41] L. Li, L. Fan, H. Duan, X. Wang, C. Luo, Magnetically separable functionalized graphene oxide decorated with magnetic cyclodextrin as an excellent adsorbent for dye removal, RSC Adv., 4 (2014) 37114–37121.
[42] P. Sharma, B.K. Saikia, M.R. Das, Removal of methyl green dye molecule from aqueous system using reduced graphene oxide as an efficient adsorbent: kinetics, isotherm and thermodynamic parameters, Colloid. Surf., A 457 (2014) 125–133.
[43] M.Z. Iqbal, A.A. Abdala, Oil spill cleanup using graphene, Environ. Sci. Pollut. Res., 20 (2013) 3271–3279.
[44] P. Bradder, S.K. Ling, S. Wang, S. Liu, Dye adsorption on layered graphite oxide, J. Chem. Eng. Data., (2011).
[45] M. McAllister, J. Li, D. Adamson, H. Schniepp, A. Abdala, J. Liu, M. Herrera-Alonso, D.L. Milius, R. Car, R.K. Prud'homme, I.A. Aksay, Single sheet functionalized graphene by oxidation and thermal expansion of graphite, Chem. Mater., 19 (2007) 4396–4404.
[46] I.A. Aksay, D.L. Milius, S. Korkut, R.K. Prud'Homme, Functionalized graphene sheets having high carbon to oxygen ratios. US patent 2011/0114897. 2011.
[47] L. Staudenmaier, Method for the preparation of graphitic acid, Ber. Dtsch. chem. Ges., 31 (1898) 1481–1487.
[48] J.C. Meyer, A. Geim, M. Katsnelson, K. Novoselov, T. Booth, S. Roth, The structure of suspended graphene sheets, Nature, 446 (2007) 60–63.
[49] F. Rouquerol, J. Rouquerol, K. Sing, Adsorption by Powders and Porous Solids: Principles, Methodology and Applications, Academic Press, San Diego, 1999.
[50] W. Gao, L. Alemany, L. Ci, P. Ajayan, New insights into the structure and reduction of graphite oxide, Nat. Chem., 1 (2009) 403–408.
[51] B. Samiey, A. R. Toosi, Kinetics study of malachite green fading in the presence of TX-100, DTAB and SDS, Bull. Korean Chem. Soc., 30 (2009) 2051.
[52] C. Moreno-Castilla, Adsorption of organic molecules from aqueous solutions on carbon materials, Carbon, 42 (2004) 83–94.
[53] J. Lyklema, Fundamentals of colloid and interface science, Volume II: Solid Liquid Interfaces, Academic, London, 1995.
[54] K. Foo, B. Hameed, Insights into the modeling of adsorption isotherm systems, Chem. Eng. J., 156 (2010) 2–10.
[55] I. Langmuir, The adsorption of gases on plane surfaces of glass, mica and platinum, J, Am, Chem, Soc., 40 (1918) 1361–1403.
[56] K. Hall, L. Eagleton, A. Acrivos, T. Vermeulen, Pore-and solid-diffusion kinetics in fixed-bed adsorption under constant-pattern conditions, Ind. Eng. Chem. Fund., 5 (1966) 212–223.
[57] H. Freundlich, Over the adsorption in solution, J. Phys. Chem., 57 (1906) 385–470.
[58] F. Haghseresht, G. Lu, Adsorption characteristics of phenolic compounds onto coal-reject-derived adsorbents, Energy Fuels, 12 (1998) 1100–1107.
[59] A. AltInIsIk, E. Gür, Y. Seki, A natural sorbent, luffa cylindrica for the removal of a model basic dye, J. Hazard. Mater., 179 (2010) 658–664.
[60] R. Han, Y. Wang, Q. Sun, L. Wang, J. Song, X. He, C. Dou, Malachite green adsorption onto natural zeolite and reuse by microwave irradiation, J. Hazard. Mater., 175 (2010) 1056–1061.
[61] Y.-C. Lee, E.J. Kim, J.-W. Yang, H.-J. Shin, Removal of malachite green by adsorption and precipitation using aminopropyl functionalized magnesium phyllosilicate, J. Hazard. Mater., 192 (2011) 62–70.
[62] H. Tang, W. Zhou, L. Zhang, Adsorption isotherms and kinetics studies of malachite green on chitin hydrogels, J. Hazard. Mater., 209 (2012) 218–225.
[63] G. Ramesha, A.V. Kumara, H. Muralidhara, S. Sampath, Graphene and graphene oxide as effective adsorbents toward anionic and cationic dyes, J. Colloid Interf. Sci., 361 (2011) 270–277.
[64] P. Bradder, S.K. Ling, S. Wang, S. Liu, Dye adsorption on layered graphite oxide, J. Chem. Eng. Data, 56 (2010) 138–141.
[65] Y. Li, Q. Du, T. Liu, X. Peng, J. Wang, J. Sun, Y. Wang, S. Wu, Z. Wang, Y. Xia, Comparative study of methylene blue dye adsorption onto activated carbon, graphene oxide, and carbon nanotubes, Chem. Eng. Res. Des., 91 (2013) 361–368.
[66] L. Fan, C. Luo, X. Li, F. Lu, H. Qiu, M. Sun, Fabrication of novel magnetic chitosan grafted with graphene oxide to enhance adsorption properties for methyl blue, J. Hazard. Mater., 215 (2012) 272–279.
[67] L. Ai, C. Zhang, Z. Chen, Removal of methylene blue from aqueous solution by a solvothermal-synthesized graphene/magnetite composite, J. Hazard. Mater., 192 (2011) 1515–1524.
[68] L. Ai, J. Jiang, Removal of methylene blue from aqueous solution with self-assembled cylindrical graphene–carbon nanotube hybrid, Chem. Eng. J., 192 (2012) 156–163.